Mekanika: Majalah Ilmiah Mekanika

3D Digital Tomography Image Reconstruction to Determine the Dimensions of Discontinuities in the Material Using MATLAB

Muhamamd Farid Azri[1], Iwan Istanto[1*], Ismail Ismail[1,2], Yuli Astriani[1,3]

1 Department of Electro Mechanic, Polytechnic Institute of Nuclear Technology, Yogyakarta, Indonesia
2 Department of Nuclear Power Plans, Tomsk Polytechnic University, Tomsk Oblast, Russia
3 School of Information Technology and Electrical Engineering, The University of Queensland, Brisbane, Australia

*Corresponding Author's email address: iwan.istanto@polteknuklir.ac.id

Keywords:
Digital radiography
Discontinuity
Tomographic
Image reconstruction
Misclassified area-mutual overlap

Abstract
To acquire more accurate information, such as the existence of discontinuities on an object from 2D digital radiography images, a reconstructed 3D image using a tomography technique is needed. In this paper, an algorithm was developed to determine the discontinuity dimension. The object used in this study is made of gypsum, which has three types of artificial discontinuities: a 4.80 mm iron ball, an 8.00 mm iron ball, and drill holes. The processes to get projection data consist of preprocessing to convert the images from red-green-blue to grayscale image format, segmentation to differentiate the object from the background using the Thresholding method and Active Contour Chan-Vese model, and morphological operations to visualize the image into 3D volumetric, followed by determining object dimensions, and subsequently the reconstruction results. The tomographic image reconstruction was constructed from 90 images irradiated by an x-ray machine using digital radiography with constant irradiation parameters and a 2° rotational angle increment interval from 0°-180°. The error results of 4.80 mm iron balls discontinuity are 1.5%, 8.00 mm iron balls are 4.1%, and drill holes are 7.05%. Moreover, the Misclassified Area-Mutual Overlap (MMO) method is employed to test the segmentation results, which resulted in an MMO value of 78.23%.

1 Introduction

Non Destructive Test (NDT) is a non-destructive testing technique on objects to determine the material properties or discontinuities contained in the object [1-3]. In the industrial world, non-destructive testing techniques are needed to determine what is inside an object. For example, an X or gamma ray with a high penetrating power technique is widely used in radiography. Nowadays, conventional radiography, which uses chemicals and old processes, has begun to be replaced by Digital Radiography (DR) [4-9]. Digital radiography is a method in advanced radiography that produces a digital analog signal for easier processing and interpretation in image processing. The digital image is generated by capturing it on a panel plate detector rather than on conventional film and is connected directly to a computer for image processing and analysis [10,11].

https://dx.doi.org/10.20961/mekanika.v23i2.85293

Revised 10 August 2024; received in revised version 18 August 2024; Accepted 4 September 2024
Available Online 23 October 2024

2579-3144

3D radiographic images have been applied in several areas, including electrochemistry [12], Medical [13,14] and engineering application [15]. A simulation study on multi-stage image registration based on list-mode proton radiography for small animal proton irradiation has been done by [16] The 3D-CT evaluation of radiographic images and the effect on diagnostic reliability of the current 2018 "Arbeitsgemeinschaft für Osteosynthesefragen"/Orthopedic Trauma Association (AO/OTA) classification of femoral trochanteric fractures have been done by [17]. A comparison of Computed Tomography (CT), Magnetic Resonance Imaging (MRI), biplanar radiography, and 3D reconstructions with and without standardized measurement training has been done by [18]. The resulting radiography image usually only shows a one-sided cross-section [19]. By its nature, one of the drawbacks of 2D radiography imaging is that it is difficult to determine the thickness or depth of an object, especially for objects with irregular geometry. Even though 3D radiography images are considered to outperform 2D imaging, they still have some limitations for specific applications. For example, in [20], the authors stated that the 2D imaging, i.e., full-mouth intraoral radiograph, provided a more accurate image for caries diagnosis for dental problems than the cone beam computed tomography-3D imaging. Furthermore, the techniques to reconstruct the one-side cross-section radiography images to a 3D imaging may result in incorrectness in some aspects, such as bias in calculating the dimension of discontinuity in the object. To address this limitation, one of the techniques that can be employed is the tomography technique, which reconstructs the projection data to produce 3D image representations. Tomography is a radiographic technique used to view the cross-section of an object. Data is obtained from the total value of transmission, emission, or reflection from various points of view. Multiple CT Slices can also be assembled to create accurate three-dimensional CT Slices that can be used for a variety of different purposes [21].

MATLAB software has used a deep transfer learning network to perform 2D-3D image construction, which can predict the deformation parameter within a statistical shape model. However, in this study, the authors emphasized that the performance of the proposed algorithm highly depended on the accurate alignment of the femoral condyles. Authors in [22] have compared the advanced iterative methods and the 3D filtered back-projection algorithm and claimed that the fast iterative shrinkage/thresholding algorithm results in a higher spatial resolution of the 3D reconstructed images. Meanwhile, in [23], 3D tomographic image reconstruction has been carried out using an algorithm program to form a 3D volumetric object as a solid rocket propellant, and the proposed program only reached the stage of propellant formation. It could not determine the dimensions and the 3D volumetric if there are discontinuities in the digital radiographic image. Moreover, the existence of discontinuity, such as localized refractive index, may cause random spikes, which then contaminate the reconstruction [24].

From those previous studies, it can be inferred that it is necessary to develop a 3D tomography image reconstruction system to determine the dimensions of discontinuities and the formation of 3D objects accurately. In this study, we created an algorithm program with MATLAB software to reconstruct a 3D radiography image and then determine the dimension of discontinuities in the object. The discontinuity dimension calculation uses a program algorithm with depth and volume parameters on three types of discontinuities with different sizes. The images in this study were taken using an x-ray machine and a rotary table with 2° shift intervals. Then, the resulting image will be acquired using Digital Radiography (DR) type DXR250U-W.

2 Experimental Methods

2.1 Material

The equipment used in this research is the Rigaku X-Ray Machine [25], Digital Radiografi-DXR250U-W [26], and Rotating Table (0-180°). The specimen used in this research is a gypsum object containing artificial discontinuities with an outer diameter of 114 mm and a height of 293 mm, as shown in Figure 1. Three iron balls with 8.00 mm and 4.80 mm diameters provided artificial discontinuity.

Figure 1. Specimen of the research

2.2 Method

The method of this research follows the diagram in Figure 2. The process starts with object projection image processing and will be finished in the testing part. A detailed discussion will be provided in the following subsection.

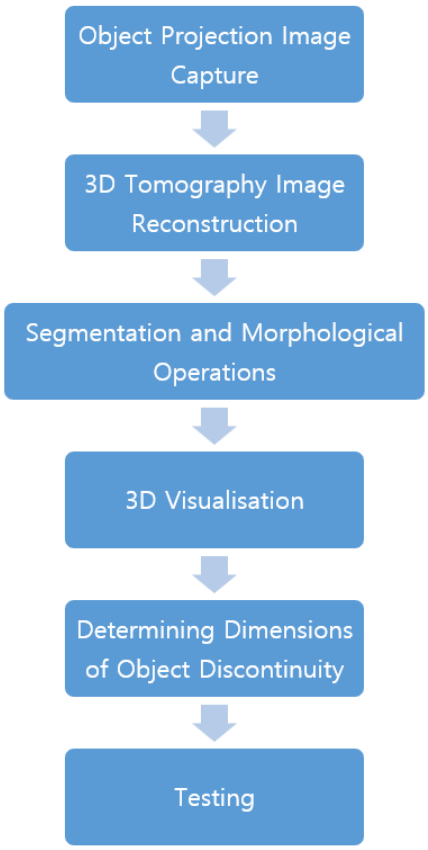

Figure 2. Experimental method

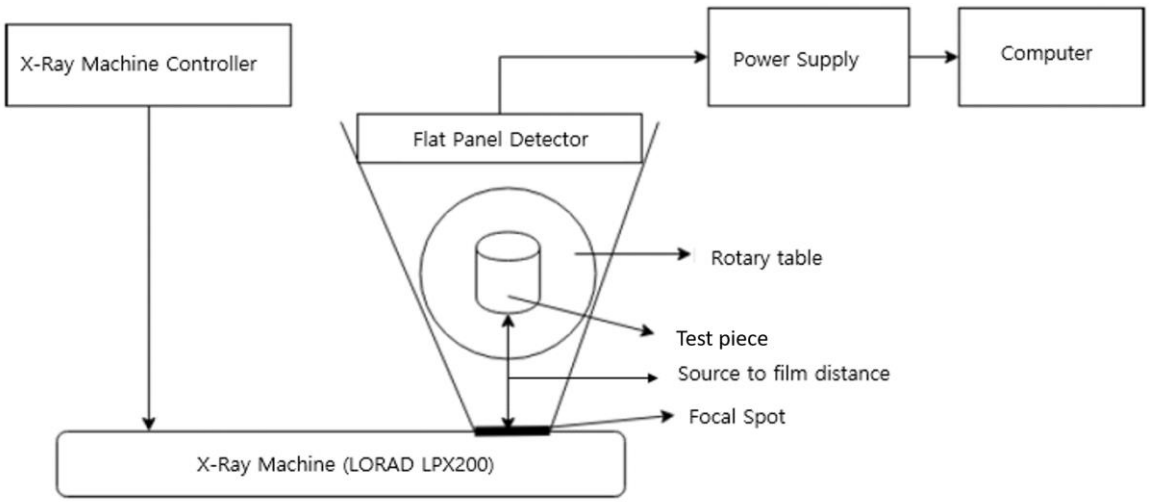

Figure 3. Equipment installation scheme

2.2.1 Object projection image capture

The tomography method [27] It was employed to acquire projection images of objects measuring 114 mm in diameter and 293 mm in height. The x-ray machine installation scheme and digital radiography settings can be seen in Figure 3. The projection data collection process was carried out at the NDT laboratory of the Indonesian Nuclear Polytechnic using a Rigaku X-ray aircraft with Digital Radiography (DR) with a DXR250U-W detector. The objects used in this research are gypsum objects that contain artificial discontinuities created by drilling into the object to a depth of 45 mm. Also, two iron balls with diameters of 8.00 mm and 4.80 mm are embedded within the objects. The projection data is captured with the source, and the detector remains in a fixed position. At the same time, the object is placed on a turntable that is rotated around the y-axis at various angles. The results of this projection data are digital images, which will be processed in the MATLAB software program to obtain 3D tomographic pictures and can be used to determine the dimensions of objects with the system.

2.2.2 3D Tomography image reconstruction

The first step in 3D tomography image reconstruction is preprocessing, which involves inputting the image reconstruction data from 90 digital projection images taken by gamma camera radiography. The next step is the CT Slice, where the radiographic image projection data is taken one slice at a time for each image to build the 3D dataset of the photos. Then, the collection of image slices will be further processed using the i-radon transformation, which will result in a sinogram image, also called an image in the i-radon domain.

2.2.3 Segmentation and morphological operations

The obtained CT Slice images were segmented using the thresholding method and active contour Chan-Vase model. This step aimed to differentiate between the object and its background so that only part of it is displayed in 3D representation. Also. This segmentation process changes the grayscale image into a binary image, where pixels only have two grayscale values, namely black (0) and white (1).

2.2.4 3D Visualization

The CT Slice segmentation results are compiled into a 3D matrix, namely the matrix for the CT Slice stack. To display it in 3D volumetric format, MATLAB's Volume Viewer application is used. The results from this application enable the analysis and measurement of the full 3D reconstruction derived from the original CT scan data.

2.2.5 Determining dimensions of object discontinuity

Determination of the location of the discontinuity is carried out on the CT Slice by observing the changes in the CT Slice. CT Slices that contain discontinuities are visible by the presence of darker parts of the object or parts with an intensity value smaller than the average intensity value of the object. This dark part is called a discontinuity. This process involves determining how many CT Slices contain discontinuities and applying segmentation to the slices that indicate discontinuities. Determination of the discontinuity volume is carried out on the segmented images and morphological results by adding up all the areas of the discontinuity section for all CT Slices where discontinuities are identified.

2.2.6 Testing

The segmentation results on the CT Slice were evaluated using the Misclassified Area-Mutual Overlap (MMO) method to indicate the discontinuity. Testing was done by comparing manual segmentation results (golden truth) with automatic segmentation. Manual segmentation was carried out using Photoshop with the author's visual indication of discontinuities, namely by classifying the discontinuity into white or black parts or as background. Meanwhile, automatic segmentation is an image resulting from segmentation that has been improved with morphological operations using an algorithm created in the MATLAB program code.

3 Results and Discussion

3.1 Object projection image capture

Projection data is retrieved using the tomography method, which involves an object image with a diameter of 114 mm and a height of 293 mm. The object used in this study is made of gypsum containing artificial discontinuities. These artificial discontinuities are made by drilling into the object with a depth of 43 mm, and there are also three iron balls with diameters of 8.00 mm and 3.80 mm in the object. The projection data retrieval process is carried out with the fixed source and detector positions. At the same time, the object is placed on a turntable that is rotated about the y-axis at various angles. Image retrieval using the tomography method is carried out by rotating the object at multiple angles using a turntable. This projection data is a digital image that will be processed using MATLAB software to obtain a 3D tomography image, enabling the determination of the object dimensions within the system.

The projection data retrieval process results are 90 projection images of the object, taken at an angle varying from 0° to 180°, with an angle increment of 2° for each step. Figure 4 shows the projection image captured at the 0° angle. The projection image of the object has dimensions of 2048 x 2048 pixels using Red Green Blue (RGB) color mode, 32-bit color depth, and in the bitmap (*.bmp) image format.

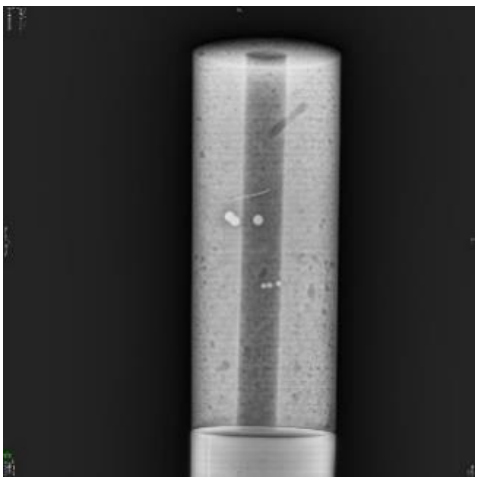

Figure 4. Image angle 0°

3.2 3D Tomography image reconstruction

3.2.1 Preprocessing

Image reconstruction was performed on 90 digital radiographic image projections. However, the digital radiographic image has a significant computational file size and needs to provide transparent information. Therefore, a preprocessing step needs to be carried out. The preprocessing process involves the following steps:

1. Equalize all projected images' dimensions by initializing the specified crop dimensions.
2. Cropping the projected image of the object to reduce the background area that is not needed for the reconstruction process.
3. Converting the original RGB image to grayscale.
4. Improving the image quality using automatic contrast stretching.

The cropping step aims to reduce the unnecessary background area for the reconstruction process and reduce the computations during image processing. This step produces a projected image of an object with dimensions of 801 x 1751 pixels, which displays only the part of the image needed in the image reconstruction process.

3.2.2 Formation of CT Slices

Image reconstruction aims to produce a CT Slice from the projected image of the object. Radiographic image projection data is taken slice-by-slice for each image and then processed into a 'sinogram' using i-radon transformation. The image reconstruction stage aims to get a cross-sectional image of the object, known as a CT Slice. The tomographic reconstruction algorithm uses the inverse i-radon transformation, i.e., the i-radon command found in MATLAB. This is considered the most direct approach for 3D image reconstruction. This i-radon command also includes a filtered back projection transformation. However, the output of iron usually results in blurred images. A filter provided in MATLAB, i.e., the Hamming filter, is employed to overcome this. This hamming filter has a slight offset value. Figure 5 shows the results of image reconstruction on the 369th CT Slice.

(a) without filter (b) with filter

Figure 5. CT Slice on the 369th

The image used in generating this CT Slice is a projected image that has gone through the preprocessing stage and consists of 801 columns and 1751 rows. Therefore, the formed CT Slice consists of 1751 images, each with a dimension of 506 x 506 pixels.

3.3 Segmentation and morphological operations

3.3.1 Object

The segmentation process uses the thresholding method to separate objects from the background in an image based on differences in brightness or darkness. The MATLAB code used to apply segmentation thresholding is “otsu thresholding,” a segmentation method by grouping where the threshold value will

automatically be obtained from the average image intensity value. Figure 6 shows the 300th CT Slice segmentation result using the thresholding command.

(a) (b)

Figure 6. (a) Results of the 300th CT Slice segmentation, and (b) Results of the 300th CT Slice morphological operation

Based on the segmentation results in Figure 6 (a), it can be seen that the object (foreground) is segmented into white (1) and the background into black (0). However, some background pixels are still segmented into white and some foreground pixels into black. Then, it is refined by morphological operations. Figure 6 (b) results from several stages of morphological operations, starting from closing, dilation, opening, and finally closing.

3.3.2 Discontinuity

1. Iron balls

The segmentation process for CT Slice indicated the presence of artificial discontinuities in the form of iron balls with a size of 4.80 mm and 8.00 mm using the Chan-Vase active contour model technique. The segmentation identified the coordinate locations where these discontinuity indications occurred within the image. This allowed the segmented regions to be isolated to the areas containing the artificial discontinuities. After that, morphological operations were performed using opening operations with different elemental structures. Figure 7 shows the segmentation and morphological process on the 1096th and 848th CT Slice, indicating a discontinuity.

(a) (b)

Figure 7. (a) CT Slice 1096th after segmentation and morphological operation, and (b) CT Slice 848th after segmentation and morphological operation

The segmented image shows that there are still a few parts of the image outside the segmented discontinuity. The segmentation results are affected by the grayscale degree of each pixel in the discontinuity area and objects. When the grayscale values between the discontinuities and nearby regions are too similar, it is difficult to determine the discontinuity boundaries. Therefore, the segmentation is carried out only in areas with a striking difference in intensity in the grayscale image.

2. Drill hole

The segmentation process for CT Slices that indicate discontinuities uses the thresholding method. This image segmentation method separates objects from the background in an image based on differences in brightness or darkness. Figure 8 shows the segmentation process on the 400th CT Slice, indicating a discontinuity.

(a) (b)

Figure 8. (a) CT Slice 400th after segmentation, and (b) CT Slice 400th after morphological operation

The segmented image still contains much noise or a small black area that should be part of the object (white), which is caused by trapped air during object creation. The image resulting from this segmentation could be better. Its structure will be corrected so it is segmented only in the discontinuity section using image morphology operations with complement, open, erosion, and "bwareafilt" operations.

3.3.2 3D Visualization

The CT Slice from the segmentation is made a 3D matrix, namely the matrix for the CT Slice stack. To display it in 3D volumetrically, this research uses an existing MATLAB application, Volume Viewer. For the formation of the 3D volume of the object taken from the CT Slice, this research employs the segmentation and morphological operations to 1751 CT Slice images. The 3D volume object display is shown in Figure 9.

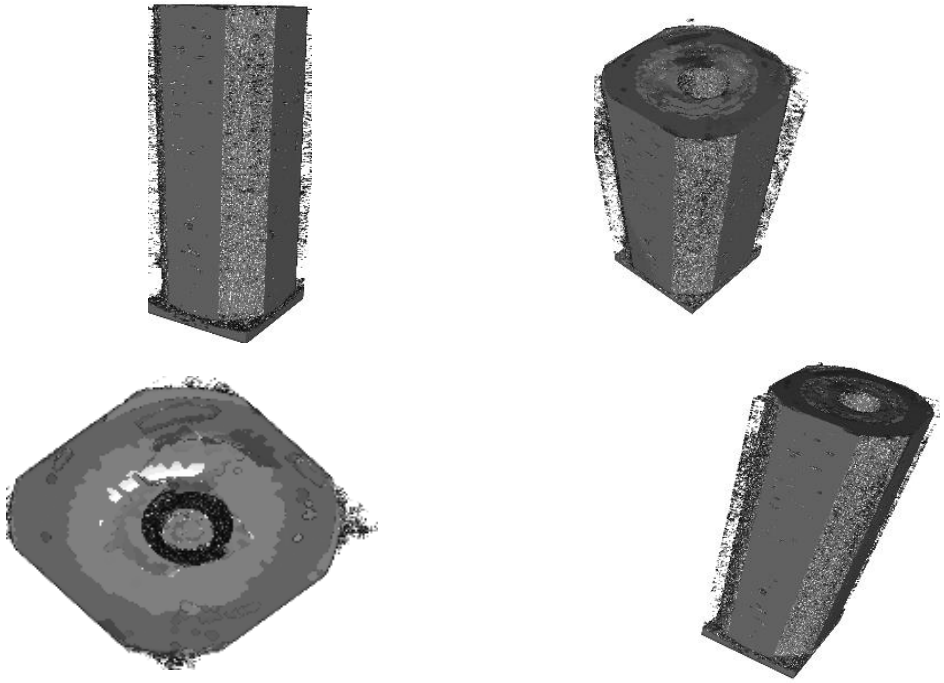

Figure 9. 3D Volumetric object with several captured angles

(a) 3D View of discontinuity of the 4.80 mm iron ball

(b) 3D View of discontinuity of the 8.00 mm iron ball

(c) 3D View of discontinuity of the drill hole

Figure 10. Volumetric discontinuity with several captured angle

The formation of 3D volumes of discontinuities from the CT Slice segmentation results and discontinuity morphology operations involves 39 CT Slice images of 4.80 mm iron balls, 51 CT Slice images of 8.00 mm iron balls, and 170 CT Slices for drill holes. The volumetric 3D view of the discontinuities is shown in Figure 10.

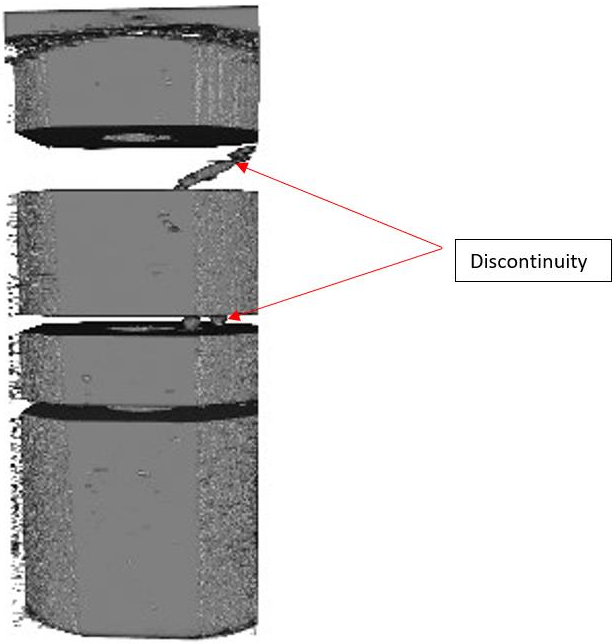

Figure 11. Volumetric object and discontinuity

The exact number of segmented and morphological images, 1751 CT Slice images, are used to construct the 3D visualization of the object and all discontinuities. The 3D visualization and discontinuities are shown in Figure 11.

3.3.3 Determining the dimensions of object discontinuities

The location of the discontinuity is determined on the CT Slice by tracking the changes in the CT Slice. The discontinuities on CT Slices are identified by the darker parts of the objects or quantified as the parts with an intensity value smaller than the object's average intensity value. Segmentation was then carried out on the slices where discontinuities were indicated. This focused the segmentation on delineating the discontinuities in the areas where they appeared. The next step is to determine the value of the discontinuity dimension in the form of the volume and depth of the discontinuity. The volume of this discontinuity is calculated by summing up the entire area of the discontinuity section for all CT Slices identified as having discontinuities on the segmented and morphological images. The discontinuity dimension generated using the explained algorithm is still in pixels. Therefore, dimensional validation is carried out to find the relationship between pixels and units of length (mm). The validation was carried out using an 8.00 mm iron ball as a reference. The validation of the discontinuity dimensions with pixel size was carried out on four iron ball CT Slices. Table 1 shows the value of the x-axis and the value of the y-axis length for each iron ball CT Slice.

Table 1. The value of the length of the x and y axes on the CT Slice of the iron ball

CT Slice	X-Axis Length (Pixels)	Y-Axis Length (Pixels)
1	48.4927	42.4075
2	47.8092	42.7426
3	47.6411	43.2932
4	46.8258	43.2207

From Table 1, the average length of the x-axis and the length of the y-axis are 47.6922 pixels and 42.9160 pixels, respectively. Therefore, the size of the depth or diameter of the iron ball obtained from the average value of the x and y-axes is 45.3041 pixels, where the value is equivalent to 8.00 mm. Thus, it is known that 1 pixel is equal to 0.1766 mm. The results of the volume determination program code show that the discontinuity volume of the 4.80 mm iron ball is 57.79 $mm^{3,}$ and its diameter is 4.94 mm; meanwhile, the discontinuity volume for the 8.00 iron ball is 251.6 mm^3 with the 8.20 mm diameter; lastly, the discontinuity volume for the drill hole is 1,128 mm^3 with a depth of 39.97 mm. These discontinuity volumes and depths are then compared to manual measurements. The percentage errors between the program algorithm results and the manual calculations were 1.5% for the 4.80 mm iron balls, 4.1% for the 8.00 mm iron balls, and 7.05% for the drill holes.

3.3.4 Testing

The test uses the Misclassified Area-Mutual Overlap (MMO) method. This method compares the results of manual segmentation (golden truth) with automatic segmentation. It identifies the area of objects that coincide in the image resulting from manual segmentation and automatic segmentation images. Automatic segmentation is a segmented image that has been improved by morphological operations using the proposed algorithm created in the MATLAB program code. The image from manual segmentation is created by manually segmenting the foreground using Photoshop software. The iron ball part is made of white color, and the other colored part is made of black color. Tests were carried out on 85 CT Slices representing all CT Slices resulting from the segmentation and morphological operations with discontinuity indications. Table 2 shows MMO data from several CT Slices, which indicated discontinuities.

Table 2 shows several results for calculating the MMO value of each tested CT Slice. The average value of MMO for all CT Slices is 78.23%. Based on the test results, there is a difference of about 12% between the results of automatic segmentation and manual segmentation. Therefore, the determination of the dimensions for the three types of discontinuities has been validated with an MMO value of 78.23%, which is declared to have passed the criteria for receiving segmentation results based on literacy from [29], which stated that MMO value should be more than 50%.

Table 2. MMO value data from the test results for each CT Slice

CT Slice	MMO (%)	CT Slice	MMO (%)
330	70.35	459	60.69
345	79.24	844	94.90
360	62.10	854	95.21
375	68.77	864	91.87
390	87.40	874	87.54
405	87.33	1095	92.77
420	90.39	1105	85.75
435	83.29	1115	88.88
Average		78.23%	

4 Conclusions

Based on the results of the 3D tomographic image reconstruction process and the determination of discontinuity dimensions, it can be concluded:

- A 3D object tomography image is generated as a stack of 1751 CT Slices displayed volumetrically.
- The resulting 3D tomography image of 4.80 mm iron ball discontinuity in the form of 39 CT Slice piles, 51 CT Slices of 8.00 mm iron balls, and 170 CT Slices drilled displayed volumetrically
- The proposed algorithm for determining discontinuity dimensions results in the iron ball's volume being 4.80 mm of 57.79 mm^3 and the depth or diameter being 4.94 mm, with an error percentage of 1.5%. The volume of the 8.00 mm iron ball is 251.6 mm^3 with a diameter of 8.2 mm, and the error percentage is 4.1%. The drill volume is 1,128 mm^3, the depth is 39.97 mm and an error percentage of 7.05%.
- The value of MMO for testing the results of image segmentation of all discontinuities is 78.23%.
- In the following research, image reconstruction is needed to determine the dimensions of natural discontinuities.

References

1. Y. E. Masri and T. Rakha, "A Scoping Review of Non-Destructive Testing (NDT) Techniques in Building Performance Diagnostic Inspections Yasser El Masri and Tarek Rakha," *Constr. Build. Mater.*, vol. 265, article no. 120542, 2020.
2. M. R. Jolly, A. Prabhakar, B. Sturzu, K. Hollstein, R. Singh, S. Thomas, P. Foote, and A. Shaw, "Review of Non-destructive Testing (NDT) Techniques and their applicability to thick walled composites," *Procedia CIRP*, vol. 38, pp. 129-136, 2015.
3. S. Kumar, M. Vishwakarma, and P. Akhilesh, "Advances and Researches on Non-Destructive Testing: A Review," *Mater. Today Proc.*, vol. 5, no. 2, pp. 3690-3698, 2018.
4. K. Kurnianto, I. M. Putra, and I. P. Susila, "Perekayasaan perangkat radiografi digital untuk industri," in *Pertemuan Ilmiah Perekayasaan Perangkat Nuklir*, Batan, Indonesia, 2013. (*in Indonesian*).

5. A. J. M. R. Sameye, A. M. Bahalkeh, and A. Izadi, "Comparison of Digital Radiography, Conventional Film and Self- Developing Film for Working Length Determination," *Iran. Endod. J.*, vol. 13, no. 3, pp. 381-384, 2018.
6. P. M. Journal and G. Bansal, "Digital radiography: A comparison with modern conventional imaging," *Postgrad. Med. J.*, vol. 82, no. 969, pp. 425-428, 2018.
7. B. Muhamedagic and L. Muhamedagic, "Digital Radiography Versus Conventional Radiography in Dentistry,"*Acta Informatica Medica*, vol. 17, no. 2, pp. 85-89, 2009.
8. M. Garmer , S. P. Hennigs, H. J. Jäger, F. Schrick, T. V. D. Loo, A. Jacobs, A. Hanusch, A. Christmann, and K. Mathias, "Conventional Radiography in Chest Imaging: Diagnostic Performance of a Large-Area Silicon Flat-Panel Detector in a Clinical CT-Controlled Study," *Am. J. Roentgenol.*, vol. 174, no.1, pp. 75-80, 2000.
9. E. Ozcete, B. Boydak, M. Ersel, S. Kiyan, I. Uz, and O. Cevrim, "Comparison of Conventional Radiography and Digital Computerized Radiography in Patients Presenting to Emergency Department," *Turkish J. Emerg. Med.*, vol.15, no. 1, pp. 8-12, 2015.
10. E. Aksit, A. Yalcin, and T. Olgar, "Effect of varying X-ray tube voltage and additional filtration on image quality and patient dose in digital radiography system," *Appl. Radiat. Isot.*, vol. 199, article no. 110893, 2023.
11. E. Ludewig, C. Rowan, K. Schieder, and B. Frank, "Journal of Equine Veterinary Science an Overview of Factors Affecting Exposure Level in Digital Detector Systems and their Relevance in Constructing Exposure Tables in Equine Digital Radiography," *J. Equine Vet. Sci.*, vol. 121, article no. 104206, 2023.
12. H. Markötter, I. Manke, P. Krüger, T. Arlt, J. Haussmann, M. Klages, H. Riesemeier, C. Hartnig, J. Scholta, and J. Banhart, "Investigation of 3D water transport paths in gas diffusion layers by combined in-situ synchrotron X-ray radiography and tomography," *Electrochem. Commun.*, vol. 13, no. 9, pp. 1001-1004, 2011.
13. S. Schafer and J. H. Siewerdsen, *Chapter 26 - Technology and applications in interventional imaging: 2D X-ray radiography/fluoroscopy and 3D cone-beam CT - Handbook of Medical Image Computing and Computer Assisted Intervention*, Massachusetts: Academic Press, 2020.
14. M. Zhang, W. Chen, S. Wang, S. Lei, Y. Liu, J. Zhang, and F. Pu, "Clinical Validation of the Differences Between Two-Dimensional Radiography and Three-Dimensional Computed Tomography Image Measurements of the Spine in Adolescent Idiopathic Scoliosis," *World Neurosurg.*, vol. 165, pp. e689-e696, 2022.
15. L. Chen, B. Li, L. Zhang, and Z. Shang, "3D positioning of defects for gas turbine blades based on digital radiographic projective imaging," *NDT E Int.*, vol. 133, article no. 102751, 2023.
16. P. Palaniappan, Y. Knudsen, S. Meyer, C. Gianoli, K. Schnürle, M. Würl, J. Bortfeldt, K. Parodi, and M. Riboldi, "Multi-stage image registration based on list-mode proton radiographies for small animal proton irradiation: A simulation study," *Zeitschrift fur Medizinische Physik*, 2023. (*in Press*).
17. M. Iguchi, T. Takahashi, T. Matsumura, R. Ae, S. Hiyama, M. Nakashima, and K. Takeshita, "Addition of 3D-CT evaluation to radiographic images and effect on diagnostic reliability of current 2018 AO/OTA classification of femoral trochanteric fractures," *Injury*, vol. 52, no. 11, pp. 3363-3368, 2021.
18. E. W. Edmonds, K. C. Parvaresh, M. J. Price, C. L. Farnsworth, J. D. Bomar, J. L. Hughes, and V. V. Upasani, "The Reliability of Measurements for Tibial Torsion: A Comparison of CT, MRI, Biplanar Radiography, and 3D Reconstructions with and Without Standardized Measurement Training," *J. Pediatr. Orthop. Soc. North Am.*, vol. 5, no. 3, article no. 661, 2023.
19. M. Amin, F. Suryaningsih, and D. Handoyo, "Perancangan Perangkat Lunak Rekonstruksi Citra 3 Dimensi Dari Lembaran Citra Hasil Rekonstruksi 2 Dimensi," *Prima*, vol. 12, no. 2, pp. 1-9, 2015. (*in Indonesian*).
20. Sumariyah, Z. Muchlisin, and E. Setiawati, "Rekontruksi Citra Tomografi Sinar-X Flouresens 2D Berbasis Teknik Radiografi Digital Menggunakan Bahasa Pemrograman Matlab 7.1," *Berkala Fisika*, vol. 13, no. 4, pp. 133-138, 2010. (*in Indonesian*).
21. J. C. Schmidt, C. Gutekunst, D. Dagassan-berndt, P. R. Schmidlin, and C. Walter, "Comparison of Two-Dimensional and Three-Dimensional Radiographs Using Clinically Relevant Parameters", *Dent. J.*, vol. 7, no. 2, article no. 50, 2019.
22. M. A. A. K. Wang, R. Su, and A. Oraevsky, "Investigation of iterative image reconstruction in threedimensional optoacoustic tomography," *Phys. Med. Biol.*, vol. 57, no. 17, pp. 5399-5423, 2012.
23. L. R. Sinta, *Pengembangan sistem rekonstruksi citra tomografi 3d pada propelan padat roket menggunakan computed radiography (CR)*, Yogyakarta: STTN-Batan, 2020. (*in Indonesian*).
24. H. G. Ha, J. Lee, G. H. Jung, J. Hong, and H. Lee, "2D-3D Reconstruction of a Femur by Single X-Ray Image Based on Deep Transfer Learning Network," *Innov. Res. Biomed. Eng.*, vol. 45, no. 1, article no. 100822, 2024.

25. Rigaku, The X-ray generator employs a ceramic X-ray tube, Rigaku. Available in *https//rigaku.com/products/imaging-ndt/ndt-products/rf-250egm2* (Accessed in July 10, 2024).
26. S. Alderton, *Digital Field Radiography Technology Update*, Boston: GE Radiography, 2014.
27. P. J. Withers, C. Bouman, S. Carmignato, V. Cnudde, D. Grimaldi, C. K. Hagen, E. Maire, M. Manley, A. D. Plessis, and S. R. Stock, "X-ray computed tomography," *Nat. Rev. Method. Prim.*, vol. 1, no. 1, article no. 18, 2021.
28. M. Sonka, V. Hlavac, and R. Boyle, *Image processing, analysis and machine vision*, New York: Springer, 2008.